ANNALI DI GEOFISICA, VOL. XXXVII, N. 5, September 1994

Seismic modeling of two depositional systems

Giuliano Brancolini ([1]), **Giuseppe Casula** ([1]), **Carla De Cillia** ([1]), **Adele Manzella** ([2]), **Alina Polonia** ([1]), **Michele Rebesco** ([1]) and **Geza Seriani** ([1])

([1]) *Osservatorio Geofisico Sperimentale, Trieste, Italy*

([2]) *C.N.R., Istituto Internazionale Ricerche Geotermiche, Pisa, Italy*

Abstract

Two ideal lithologic sections representing a tidal bar system and a fluvial complex were drawn in order to run seismic modeling programs developed by OGS on behalf of the European Community. The simulations allowed an accurate analysis of the seismic expressions of the two sections. The tidal bar system is formed by a number of sandstone lenses interlayered with siltstone and mudstone deposits. These lenses meet together on an erosion surface, while they thin and vanish in the other direction. The fluvial complex is formed by a limestone basement overlain by coarse alluvial plain sediments which in turn are transgressed by finer flood plain sediments, including sandstone lenses stacking towards the top in a meandering belt. These lithofacies associations represent potential multi-pool reservoirs in which the mudstone layers constitute the plugs. As a function of the granulometric and depositional features of each lithological unit, together with fluid content, wave velocities and densities were evaluated. A 2D modeling for elastic plane wave propagation in these hypothesized geologic sections was run on a Cray supercomputer. The numerical scheme is based on solving the full wave equation by pseudospectral methods.

Key words *seismic modeling – depositional systems – tidal bars – fluvial complex – wave equation*

1. Introduction

As seismic sections strongly influence geologists' stratigraphic ideas, it is more and more important to know both the seismic limitations and how this method succeeds in representing the subsurface geology.

Biddle *et al.* (1992) produced a seismic model of a progradational carbonate platform starting from a detailed lithologic cross section obtained from a well-exposed Triassic succession at Picco Vallandro in Northern Italy. Even though a very simple monodimensional modeling tecnique was adopted, some relevant discrepancies between the geologic and the seismic sections were pointed out. In particular, the backstepping periods of the platform margin could be interpreted, in the seismic model, as an unconformity surface formed during a relative sea-level fall with later onlaps of a transgressive cycle. Likewise, the seismic downlap does not correspond to discrete stratal surfaces, but to the toe-of-slope position, where major bedding units thin below seismic resolution. They concluded that, with the seismic section alone, it would be possible to reconstruct a history that does not correspond to that seen from the outcrops.

Noah *et al.* (1992) presented a 3-D seismic model of channel point-bar deposits and four 2-D normal incidence synthetic lines. An apparent lack of correlation between seismic amplitude and sand thickness shown by these ray-traced lines is due to Fresnel zone effects, which may also lead to misinterpretations of the actual position of the channel edge on oblique crossing lines. Interpretation difficul-

ties can arise from spatial separation between a number of different point bars. The wide degree of interpreter subjectivity in mapping the sand bodies under investigation is also demonstrated. The interpreter's knowledge, in fact, is the basis for the geological scenarios of seismic modeling.

Rebesco and Polonia (1993) discussed the synthetic traces obtained from detailed geological sections of a tidal bar sequence. A reflection coefficient series, derived from the assigned velocities and densities to each geological facies, was convolved with a set of band-pass filters. The effect of various earth filters and acquisition parametres was thus analysed by means of noise-free high resolution and poor quality narrow-band synthetic traces. Only the high resolution (8-300 Hz) seismic wavelet was able to represent most of the details of the geological sections.

2. The geologic model

Two examples of geologic environments, representative of a tidal and an alluvial plain, were considered.

Tidal deposits (Mutti *et al.*, 1985 and more general situations in Postma, 1967) have a cyclic character due to flood and ebb opposite direction currents. For a better comprehension of this kind of phenomena we describe below

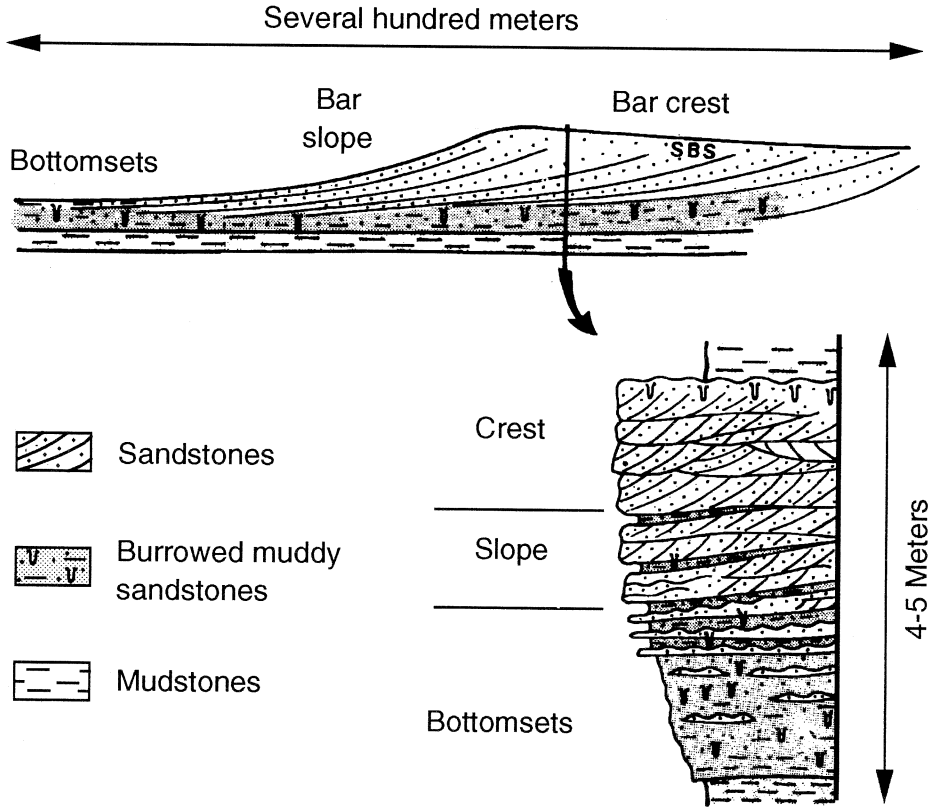

Fig. 1. Schematic representation of a tidal bar and its stratigraphic column (SBS = sigmoidal bed set) (from Mutti *et al.*, 1985).

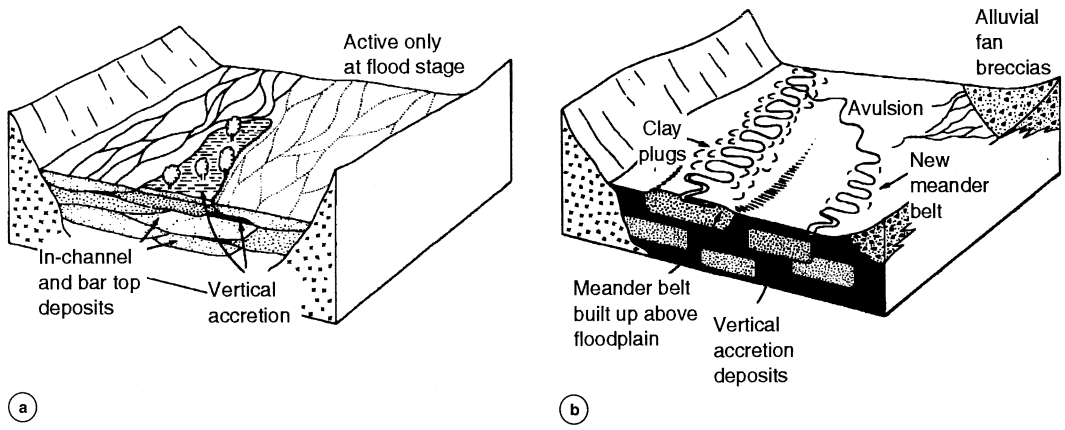

Fig. 2a,b. Block diagram of the two fluvial complex end-members: a) braided system with low sinuosity channels; b) flood plain aggradation with a meandering river (from Walker, 1984).

the small scale processes and resulting centimetric structures which are well studied at the outcrop scale. A similar cyclic character is also present in larger scale geological bodies, controlled by higher rank periodicity.

These outcrop-scale deposits are primarily produced by the propagation of tidal waves which generate two opposite currents alternating about every six hours at any given site. The strength of these currents is related to the tidal range, which is increased by constrictions such as in estuaries and in some shelf areas.

The intensity of these currents has a typical sinusoidal trend: each semidiurnal cycle is composed of a rising and falling tide, and during every phase the velocity increases, reaches a maximum and then decreases. During the high velocity stages, coarse sediments can be moved giving rise to cross bedded deposits (centimetric scale). During slack periods (points of current reversal), no water mass movement occurs and finer suspended sediments may settle and cover the sigmoidal sand bodies with mud drapes.

In every tidal cycle, sediment undergoes a cycle of erosion, deposition and transport in opposite directions. Hence in tide dominated areas, sediment is continuously subjected to a cyclic reworking under conditions of varying energy levels. This frequently results in the typical features of tidal deposits (fig. 1): bidirectional structures (herringbone cross-stratification), although only locally abundant and normally replaced by predominant current direction structures with smaller scale subordinate features; repetitive sand-clay interlayering units; sigmoidal cross-bed geometry.

Fluvial deposits (Walker, 1984) generally consist of flood plain sediments and river-sand bodies, whose external geometry is given by a downward erosive surface cutting underlying strata. Single channels may be associated together in space and time giving rise to more complex depositional structures formed by a succession of several events. These structures may have various features, but the two main cases are due to braided and meandering streams (fig. 2a,b).

Braided channels are normally associated with high gradients (upper flood plain) and consist of multiple channels bounded by bars, which frequently change their position. Deposits (fig. 3a) consist of pebble, gravel, sand and subordinate clay; they are lenticular and discontinuous due to repeated erosion, and each cycle corresponds to a flood event.

Meandering channels occur in lower alluvial, coastal and deltaic plains. In comparison with the braided system, the channel is single and deeper and sediments are finer (fig. 3b).

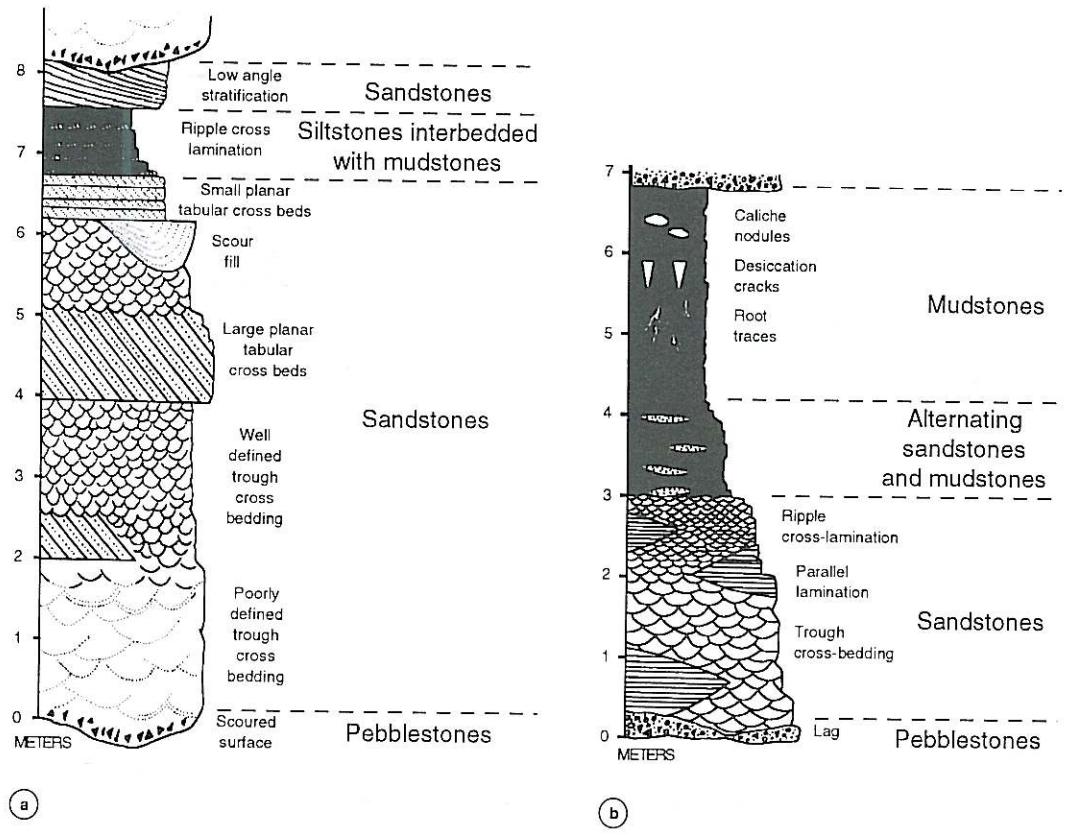

Fig. 3a,b. a) Sequence representing the typical facies relationship of a braided system (data from Devonian Battery Point Sandstone, Quebec); b) sequence for lateral and vertical accretion deposits of meandering rivers (data from Devonian Old Red Sandstone of Britain and Catskill rocks of the Eastern U.S.A.) (from Walker, 1984).

The channel migrates laterally within a zone 15-20 times wider than the channel itself, giving rise to the meander belt elongated sand body; the meander belt may upgrade on the flood plain and generate a stacking of sand bodies. The meander belt is bounded by the natural levees and by the flood plain deposits, consisting of organic-rich clay with laminated silt lenses.

3. Physical parametrization of the model

Starting from the general features of the tidal bar and the alluvial plain systems, two petrophysical schemes have been constructed. They can be regarded as a simplified lithological cross-section in which the main external and internal geometry of the two environments have been represented.

The tidal bar scheme (fig. 4) is 2 km long and 500 m thick. The lower part, below a surface dipping towards the right, consists of limestone strata which are tilted and eroded.

The tidal-bar complex occupies the central part of the section, directly overlying the limestone on the left side. This complex is composed of sandstone lenses prograding towards the right. They are stacked, on the left, forming

a single body containing a few siltstones, while, on the right, they are separated and enclosed by the finer siltstone sediments which plug the whole system.

The upper part of the scheme contains a second erosional surface, slightly undulating, two more sandstone lenses buried within mudstone deposits, and some other muddy siltstones overlying a third deeply incised surface.

The second scheme (fig. 5) is 5 km long and 500 m thick. It represents a fluvial deposit system in which the lower part is constituted by upper flood plain sediments belonging to a braided channel system, and the upper part is occupied by fluvial sediments enveloped in fine flood plain deposits that upgrade and, towards the top, migrate laterally.

The upper flood plain is constituted by the conglomerates of a braided river, including only few sandstone lenses, and overlying a limestone basement with an alluvial fan covering.

Over an almost even transgressive surface, the finer lower flood plain sediments include coarse deposits of a braided fluvial channel, becoming sandy upward and finally evolving to a stacked sandstone belt with some siltstone lenses of a mature meandering river. The upper leftmost part of the meandering belt is gas mineralized with an even horizontal gas-water contact surface below it.

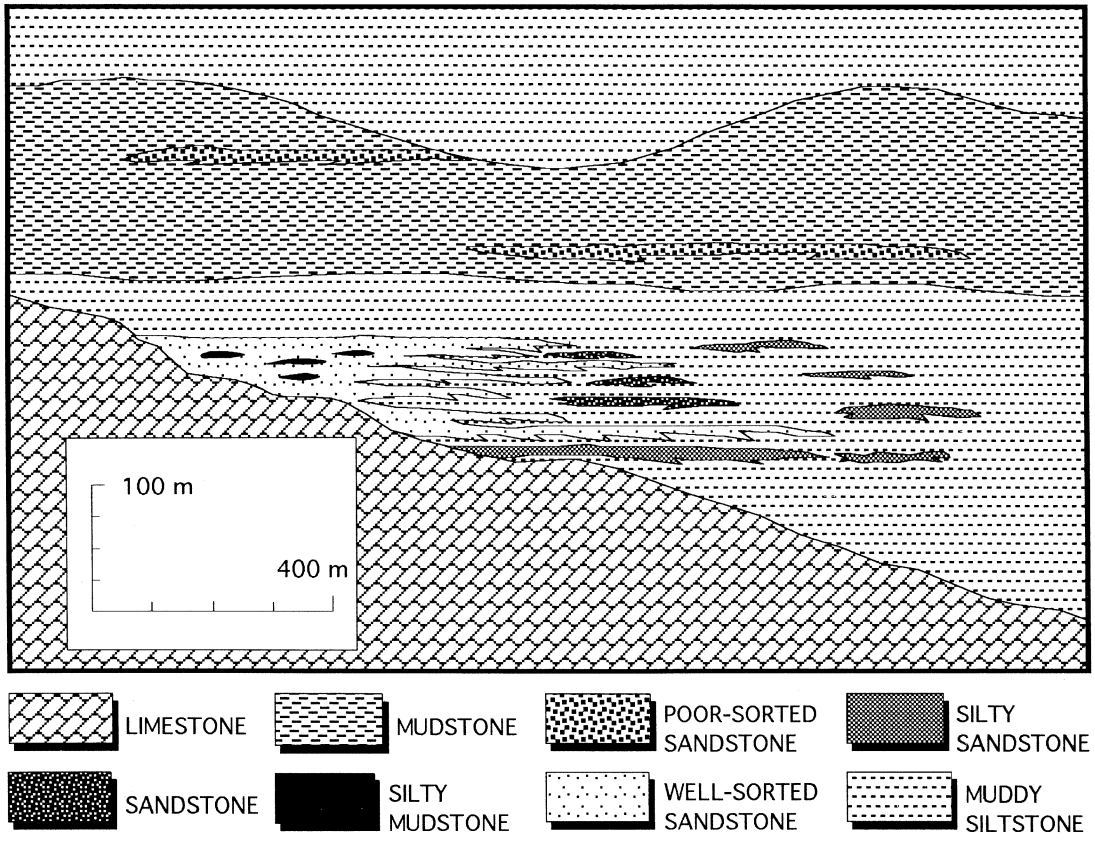

Fig. 4. Geologic section of an idealized tidal bar system.

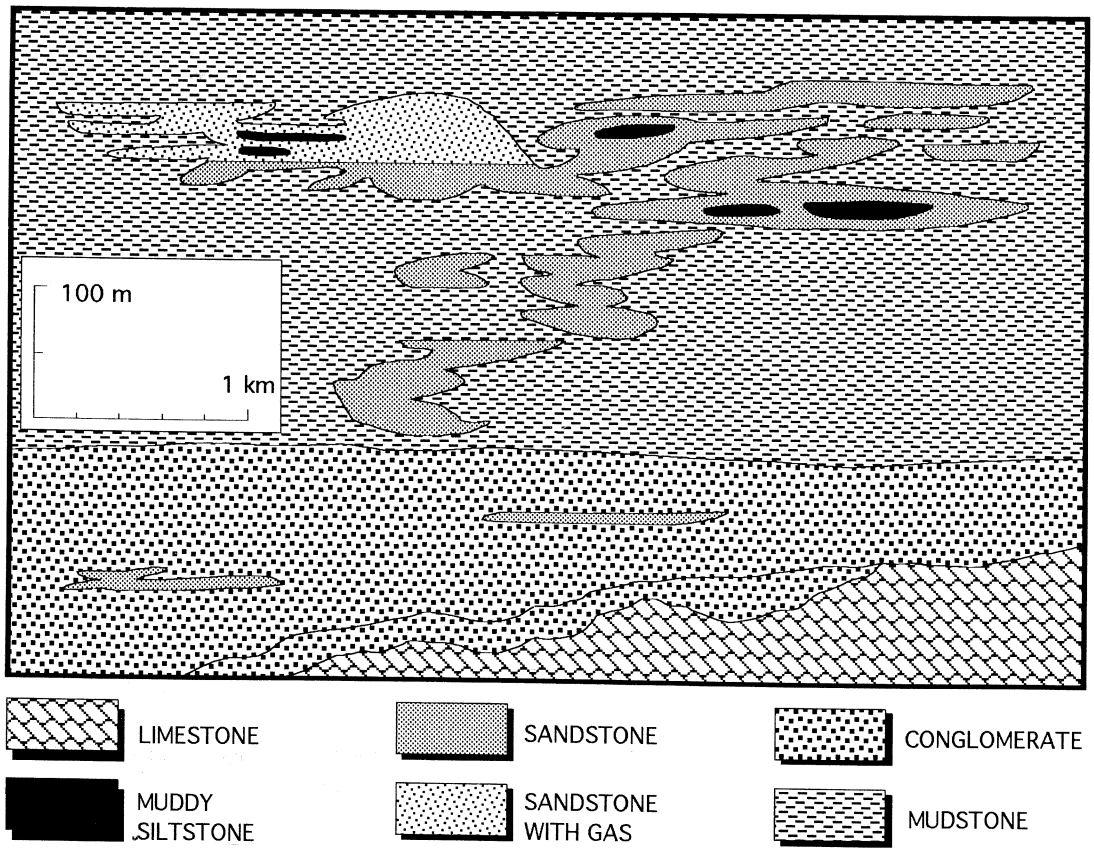

Fig. 5. Geologic section of an idealized fluvial complex.

As a function of the lithologic, granulometric and depositional features of the different facies, and fluid content, *P* and *S* wave velocities and densities were assigned on the basis of the laboratory measurements on rock samples with similar petrophysical features obtained from Han *et al.*, 1986 (see tables I and II). The large seismic velocity range of the sandstones reflects the evolution of the river system from braided through to meandering.

In this operation, we inevitably insert a certain degree of subjectivity and a margin of error, due to the lack of direct velocity measurements, but for an impedance model, only the relative velocities, and not the absolute values, need be considered.

In the following tables, the lithotypes considered, the corresponding *P* and *S* wave velocities, and the density are represented.

4. The seismic model

The 2D modeling utilizes the discrete grid method based on solution of the full wave equation which, without any simplification of physical assumptions, allows for an easy and accurate model definition from both the geometric and physical points of view, whatever the complexity of the geologic structure under investigation.

These two points are very important be-

Table I. Tidal model velocities and densities.

Lithotipe	*VP* (m/s)	φ (gr/cm^3)	*VS* (m/s)
Limestone	4500	2.45	2600
Well-sorted sandstone	4300	2.34	2500
Sandstone	4000	2.34	2350
Silty sandstone	3800	2.34	2200
Poor-sorted sandstone	3400	2.34	1950
Muddy siltstone	2900	2.34	1700
Silty mudstone	2600	2.34	1500
Mudstone	2500	2.34	1450

Table II. Fluvial model velocities and densities.

Lithotipe	*VP* (m/s)	φ (gr/cm^3)	*VS* (m/s)
Limestone	5000	2.45	2900
Conglomerate	4500-4600	2.35	2600-2650
Sandstone	3300-4400	2.34	1900-2550
Sandstone + gas	2800	2.34	1600
Muddy siltstone	2900-3300	2.30	1700-1900
Mudstone	3000	2.25	1750

cause the techniques take into account all the complex phenomena of wave propagation, be they primary, reflected or refracted waves, multiple reflections, surface waves, head waves, converted waves and diffracted waves. The most widespread of these methods are the finite difference (FD), pseudospectral or Fourier (FS) and finite element (FE) methods (Kelly *et al.*, 1976; Marfurt, 1984; Kosloff *et al.*, 1984; Fornberg, 1987; Seron *et al.*, 1987; Seriani and Priolo, 1991; Seriani *et al.*, 1992).

Even though based on different mathematical approaches, all three methods rely on space discretization of the geological structure to be modeled. In particular, solution of the wave equation is computed at the nodes of the space mesh for each time step, while the time evolution is usually computed using a finite difference discretization, which is equivalent to computing the wavefield at a fixed time interval Δt.

The model is specified by associating to each node the density (φ) and Lamé parameters (μ and λ), or the pressure and shear velocities (*VP* and *VS*).

With all these methods, wave propagation must be simulated for an unbounded spatial domain (the Earth) using a finite domain, due to the restriction of computer resources; hence the numerical treatment of the boundary conditions is a crucial point that can be faced by imposing absorbing strips in the vicinity of the model boundaries: the energy of the incident waves is assumed to be totally absorbed by these strips, allowing for no back reflections (Cerjan *et al.*, 1985). It must be noted that this is an easy problem to solve in the case of a homogeneous lithotype, but it become very difficult in practice when different lithotypes are involved. These strips act as a further lithotype that must absorb the energy, avoiding reflection events which are almost impossible to eliminate when more than one lithotype (with

different physical properties) are in contact with the absorbing strip. In this case, for the parameters defining the absorbing strips, an average value must be chosen in such a way as to allow maximum absorption of the out-going energy, minimizing spurious reflections in the various lithotypes. The deeper feeble event in figs. 7 and 9 is in fact caused by the absorbing strip.

The computational complexity and accuracy of the results are strongly dependent on the choice of characteristic length (Δh) of the single elements or cells of the spatial mesh, and on the time integration step (Δt).

The minimum values of the parameters Δh and Δt are thus restricted by computing power and cost, while the maximum values are restricted by:

- the minimun spatial dimensions of the geologic structures present in the model;
- the requirement of no numerical wave dispersion;
- the stability condition of the numerical model;
- the frequency bandwith of the source.

The importance of correct choices of Δh and Δt must be stressed, since wrong choices can produce unwanted effects. A numerical model for the study of the wave propagation phenomena can be seen as a low-pass filter, since low frequencies (wavelength large compared to grid size) propagate correctly, while high frequencies (wavelength small compared to grid size) do not propagate well. At high frequencies, the possible unwanted phenomena that can be produced are:

- wave attenuation or amplification;
- numerical anisotropy; that is the propagation velocity is dependent on the direction of the incident wave with respect to the orientation of the grid;
- wave dispersion and polarization;
- errors in phase and group velocity;
- numerical parasitic wave generation.

In the present work, pseudospectral and finite element methods were used. The first is based on a Fourier expansion of the wave field to be computed solving the differential wave equation, while in the second the wave field is obtained as a sum of the local element solution of a weighted residual minimization problem equivalent to the original wave propagation problem.

The numerical models were run on a Cray Y-MP supercomputer using 25 Mwords of central memory. As a source we used a plane wave impulsive source with 150 Hz peak frequency and 300 Hz cutoff frequency.

The synthetics corresponding to the results obtained with the two methods are indistinguishable. The pseudospectral seismic sections of the two idealized geologic sections are shown figs. 6 and 7. In figs. 8 and 9 the synthetic data have been convolved with a zero phase 8-50 Hz bandpass filter and a certain percentage of white noise added. Sections in figs. 6 and 7 can be regarded as theoretical results of very good quality, high resolution seismic data while sections in figs. 8 and 9 are representative of rather poor quality data.

5. Discussion

The aim of the experiment was:

- to test the efficiency of the modeling programs developed by the OGS research group;
- to produce the seismic expression of some depositional environments that could be useful in seismic data interpretation.

Only the second point will be discussed in the present paper, since the first is essentially addressed to the computational aspects of the problem.

The conventional seismic polarity has been adopted to plot the modeling results: a positive reflection coefficient is a negative number and corresponds to a white trough on the synthetic sections while a negative coefficient corresponds to a black peak.

Comparing the tidal bar system in fig. 4 and the seismic section in fig. 6, we notice that the former is quite well represented: the external shape is perfectly preserved and most of the in-

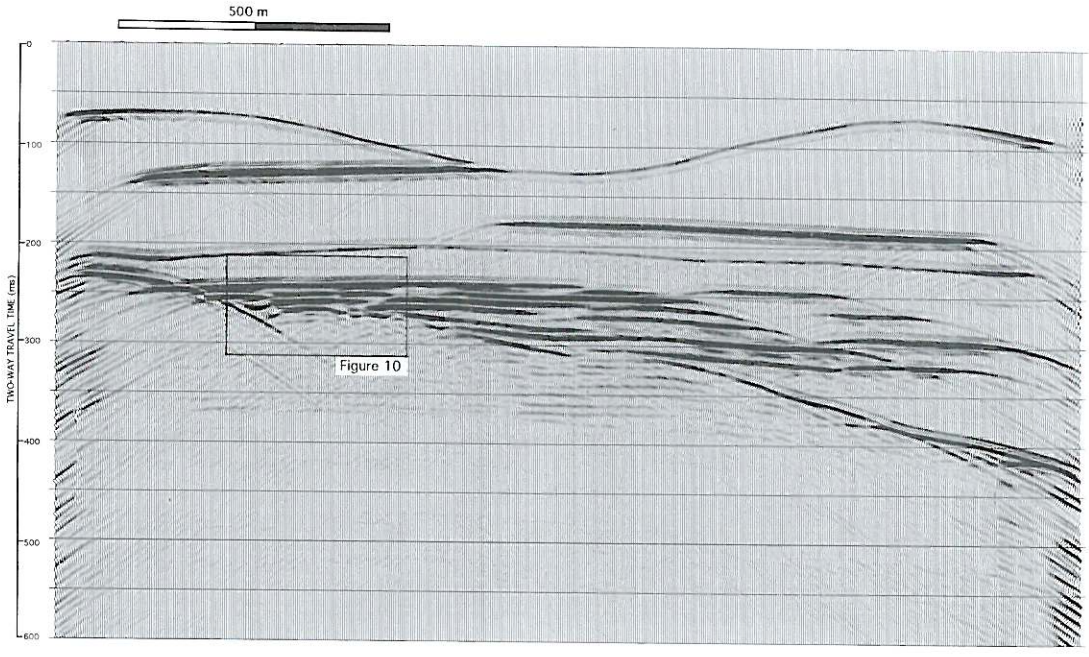

Fig. 6. Synthetic seismic section of the tidal bar system obtained from an elastic plane wave propagation modeling of the geological section in fig. 4. The model was run on a Cray supercomputer solving the full wave equation by pseudospectral methods.

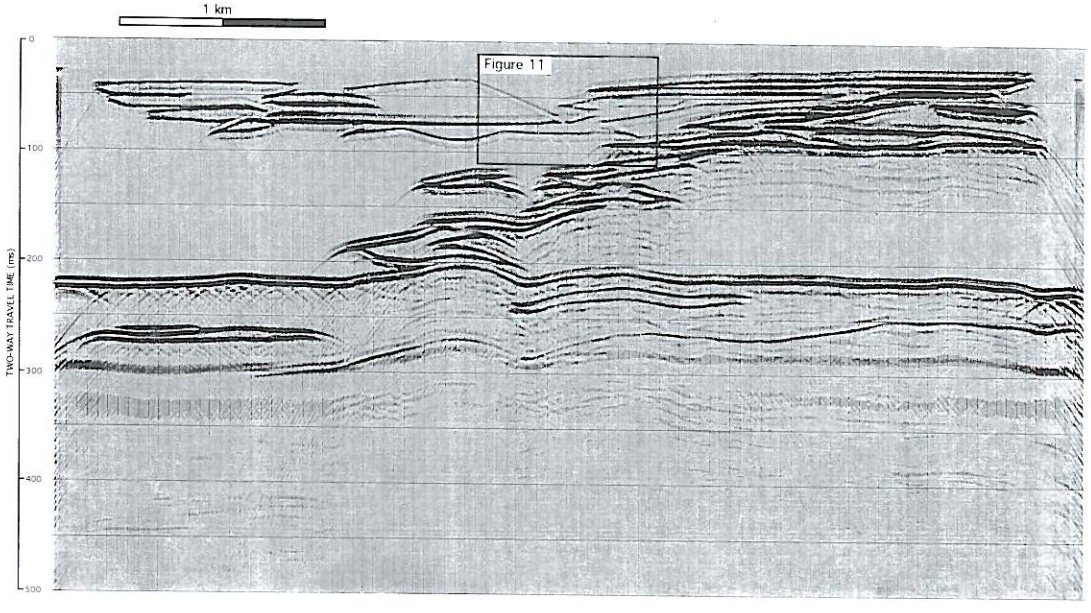

Fig. 7. Synthetic seismic section of the fluvial complex in fig. 5. The same method, source and supercomputer of the model in fig. 6 were used for this simulation.

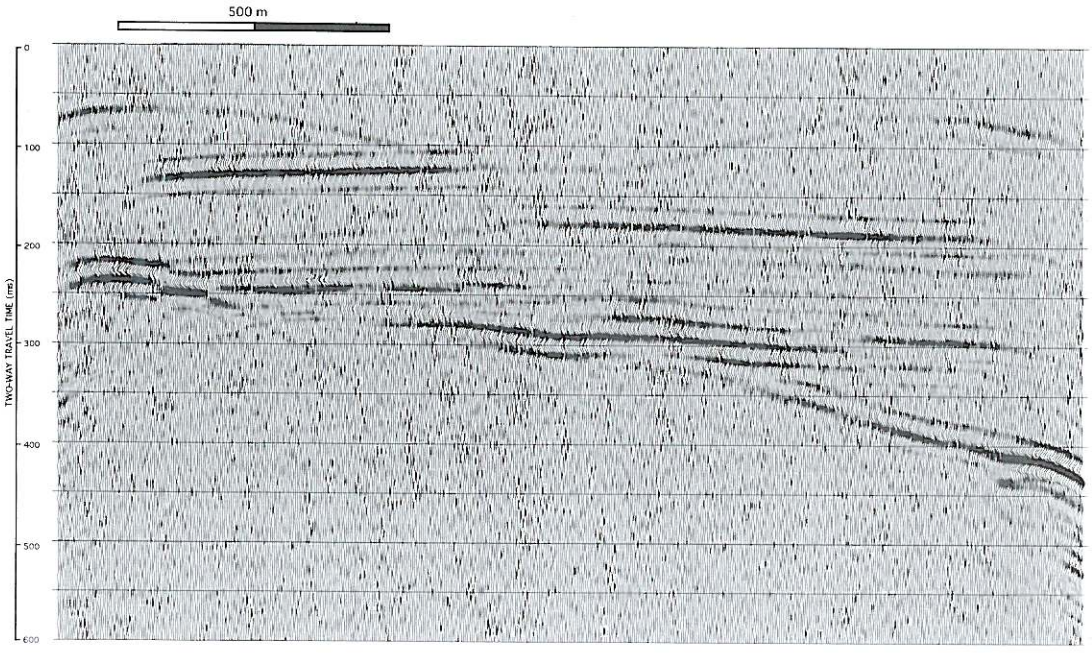

Fig. 8. Filtered version of the model in fig. 6. It simulates a poor-quality 4-ms-sampled seismic section. Data of fig. 6 have been bandpass filtered (4-8 / 50-80 Hz) and random noise added.

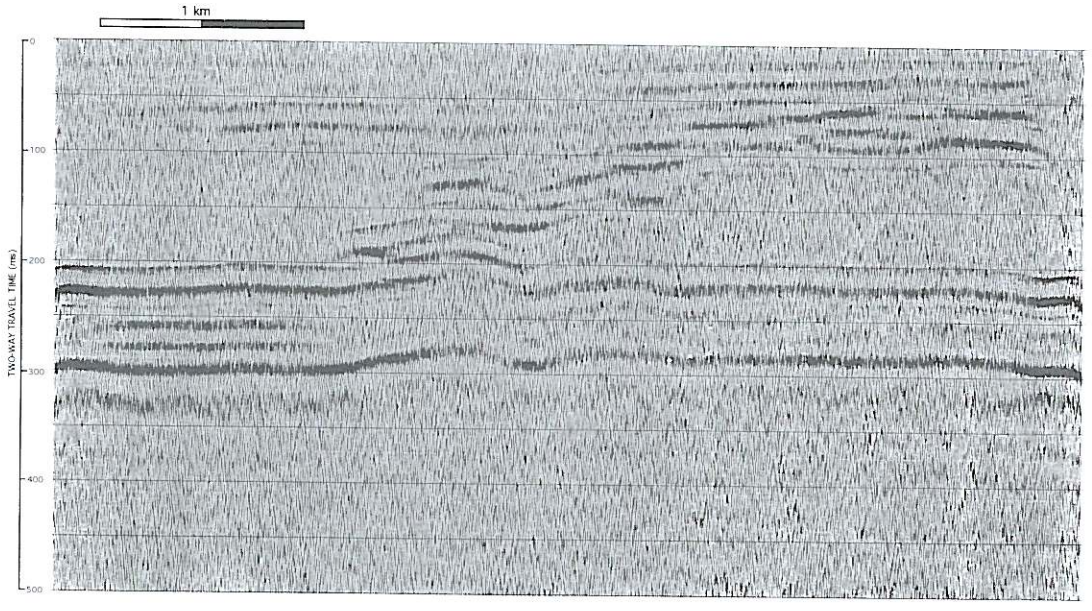

Fig. 9. Poor-quality seismic section simulation of the model in fig. 7. The bandpass filter and the random noise percentage are the same as in fig. 8.

ternal features are fairly well recognizable. Nevertheless, some peculiar limits of the seismic section that can easily produce misleading interpretations must be discussed.

However before entering into an analysis of the experimental results, it would be useful to consider vertical resolution in seismics.

Widess (1973) produced synthetic traces starting from two spikes of equal amplitude but opposite polarity convolved with different zero phase wavelets. He observed that the spikes produced totally distinguishable reflections when they were separated by more than an half of the wavelength of the incoming wave. Below 1/2 of the wavelength the two reflections start to interfere but, for distances between 1/2 and 1/4 of the wavelength, it is still possible to resolve the two spikes. When the distance is around 1/4, the interference between the wavelets produce a «tuning» effect that increases the amplitude of the resulting wavelet. Below 1/4 of the wavelength the two spikes are not directly resolvable, only the tuning effect, which is proportional to the distance between the spikes can be used, at least theoretically, for evaluating the possible presence and the thickness of a thin layer. As the spike distance approaches 1/8 wavelength the interference is destructive and the amplitude decreases. Below 1/8 the shape stabilizes while the amplitude decreases almost linearly with the distance between the spikes. Similar considerations also apply to minimum phase wavelets.

Coming back to our synthetic section (fig. 6), we notice that the first arrival produced by the uppermost erosional unconformity is a black peak: which is in agreement with the velocity inversion due to the higher velocity of the muddy siltstone underlying the slower mudstone.

The two poorly sorted sandstone lenses inside the mudstone in the upper part of the model are rather well resolved. Even if the lens boundaries do not give two separate reflections, it is still possible to calculate the thickness of the lenses starting from the «trough to peak» distance, whose maximum value is about 3.5 ms; multiplying this value by the interval velocity (3400 m/s) and dividing it by two, we obtain 8.15 m, which is in very good agreement with the real thickness (8.5 m). The polarity of the first arrival from the top of the lenses is a white trough; which implies, considering that the contribution of the density in the reflection coefficient is negligible, an increase in the *P*-wave velocity. Notice that the interference between the two minimum phase wavelets produces a composit wavelet whose shape is very similar to a zero phase wavelet.

Another remarkable effect of the interference is the high amplitude of the black peak compared to the much lower amplitude of the white trough. This phenomenon, caused by the positive interference between the second leg of the wavelet from the top of the lenses with the first leg from the bottom, gives the reflection an apparent negative reflection coefficient, which could easily lead to a misinterpretation of the seismic data.

The tidal bars develop below the second erosional unconformity at about 200 ms, and the unconformity marks an increase in the *P*-wave velocity from 2500 m/s to 2900 m/s. The first reflection at about 240 ms to the left of the seismic section is the consequence of a strong velocity increment (muddy-siltstone overlying well-sorted sandstone).

The small silty-mudstone lenses (A, B and C in fig. 10) inside the well-sorted sandstone have an average thickness of 3 m, which is less than 1/4 of the wavelength. That means that the lenses are not resolvable on our seismic section; however even in this case, some considerations on the seismic character of this part of the section can help for a correct interpretation of the data.

Two of the lenses under examination (A and C) are rather close to the uppermost boundary of the well-sorted sandstone. Their presence produces a «bright spot» effect and a lowering of the apparent frequency in the black peak of the sandstone reflection; the black peak is followed by a pronounced white trough and a similar amplitude peak.

The two other lenses are superimposed over each other (the upper is indicated as B in the close-up of fig. 10) and are well separated from the top of the sandstone. The real polarity of the reflections, which starts with a black

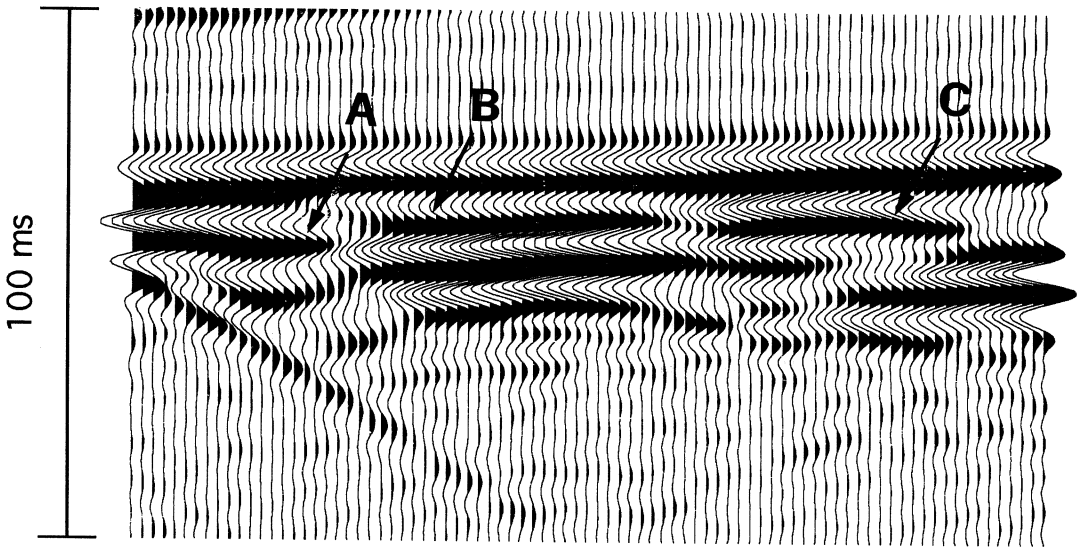

Fig. 10. Close-up of part of the synthetic seismic model of the tidal bar system (position indicated in fig. 6). Letters A, B and C refer to the arrowed silty-mudstones lenses discussed in the text.

peak, is rather evident in this case, and it is relatively easy to predict the presence of low velocity lenses.

Moving to the central part of the section, the interfingering of the well-sorted sandstone with the mudstone causes a progressive increase in the number of low and high velocity layers. Most of the strata are below the resolution limits of our model and the resulting picture is therefore quite confused, and it is not possible to get any idea of the velocity distribution.

On the right side of the section, the silty-sandstone lenses are completely isolated and well resolved. In this case the velocity increment is evident from the polarity of the first arrival.

The tilted and eroded limestone basement causes focussing and diffraction phenomena in the incident wavefront. The erosional surface is represented by a rather discontinuous reflection. Some of the discontinuities could easily be misinterpreted as faults, and artificial structural elements thus introduced into the interpretation.

If the quality of the seismic data becomes poor, as in the example of fig. 8, where an 8-50 Hz bandpass filter and a certain amount of white noise has been applied to the seismic model, most of the previous considerations are no longer valid.

The adopted filter, in fact, produces an increase in the signal wavelength, and therefore the seismic data resolution decreases. As a function of the interval velocities, the wavelength now ranges between 20 and 30 m. As a consequence, in the tidal bar model section of fig. 9, all the lenses are below the resolution. Only for the two isolated lenses in the upper sequence is the prevalent negative reflection polarity and therefore the velocity increase still recognizable. Thus as the quality of the seismic section deteriorates, only the external shape of the tidal bars can be inferred.

The synthetic seismic section of the fluvial complex (fig. 7) can be analyzed with the same criteria as the tidal bar system. Resolution in fact is high enough to distinguish all the lenses and the lateral relationships between different lithotypes. The pull-up effects in the central

part of the section are interesting. Between traces 300-450 and traces 500-600, in fact, the top of the conglomerate of the braided alluvional plain presents two anticlines that are not part of the geological section. The same structures can be observed in the sandstone lens inside the conglomerate (traces 500-600) and the top of the carbonates in the deepest part of the section.

The origin of the structures is the pull-up effect caused by the overlying sandstone body, whose seismic velocity is higher than the velocity of the surrounding mudstone.

This pull-up effect is quite a common source of error in seismic interpretation and can produce great problems in hydrocarboon exploration because it simulates pseudo-anticlinal structures. An accurate evaluation of stacking velocities and an appropriate depth migration of the data can generally resolve most of the practical situations. In any case, seismic modeling techniques are very useful for support and/or verification of the results.

On the left side of the upper part of the model a sandstone lens with gas has been simulated. The presence of gas has the effect of decreasing the *P*-wave velocity and reducing the acoustic impedance contrast. In our case the decrease in acoustic impedance in the sandstone lenses led to inversion of the reflection coefficient. The presence of the gas is easily recognizable by the polarity inversion of the reflection from the uppermost boundary of the lens (fig. 11).

Following the same procedure as for the tidal model, the fluvial model section was bandpass filtered (8-50 Hz) and a certain percentage of white noise added (fig. 9). Also in this case the results are very similar to a poor quality seismic section. The external shape of the bodies is still preserved but no seismic-stratigrafic deductions are possible. The lack of resolution and the low signal-to-noise ratio have destroyed all internal features of the depositional environment.

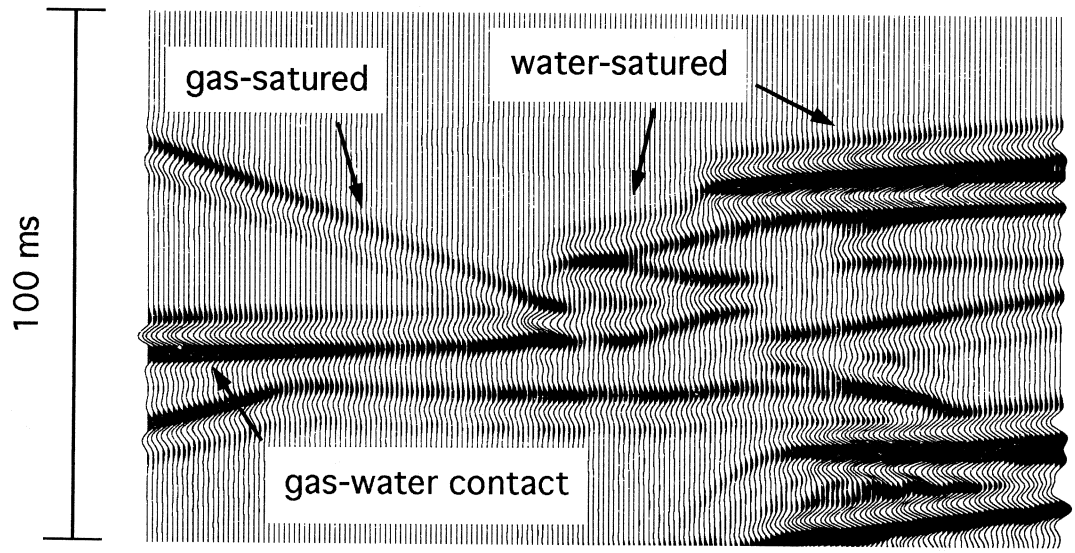

Fig. 11. Close-up of part of the synthetic seismic model of the fluvial complex (position indicated in fig. 7) showing the different seismic characters of a sandstone lens partly gas-satured (left) and partly water-satured (right).

6. Conclusions

The seismic modeling of two depositional settings provided an opportunity to evaluate how seismic techniques succeed in representing such environments: bright spots and polarity inversions due to thin-bed tuning effects, and artifacts in the basement structural style have been demonstrated in the tidal bar model, whereas pull-up and gas effects were recognized in the fluvial plain model.

Seismic modeling techniques are thus an efficient tool for improving seismic interpretation reliability.

Some preliminary conditions, however, should be respected:

a) geological and geophysical knowledge should be detailed enough to handle much of the complexity of the geological situations, and should be based on at least one direct source of information (for example a well);

b) modeling programs should take into account all the physical parameters that characterize the earth filter (anisotropy, transmission losses etc.);

c) harder configurations should allow a multi-coverage and interactive seismic simulation to be run.

The most promising applications of such techniques are thus found in the oil industry for reservoir studies.

Acknowledgements

The research was funded by contributions from the E.C. under the EOS and Artificial Intelligence Programs in the framework of the JOULE Program.

REFERENCES

BIDDLE, K., W. SCHLAGER, K. RUDOLPH and T. BUSH (1992): Seismic model of a progradational carbonate platform; Picco Vallandro, the Dolomites; Northern Italy, *Bull. Am. Assoc. Pet. Geol.*, **76**, 14-30.

CERJAN, C., D. KOSLOFF, R. KOSLOFF and M. RESHEF (1985): A non reflecting boundary condition for discrete acoustic and elastic wave equations, *Geophysics*, **50**, 705-708.

FORNBERG, B. (1987): The pseudospectral method: comparisons with finite differences for the elastic wave equation, *Geophysics*, **52**, 483-501.

HAN, DE-HUA, A. NUR and D. MORGAN (1986): Effects of porosity and clay content on wave velocities in sandstone, *Geophysics*, **51**, 128-142.

KELLY, K.R., R.W. WARD, S. TREITEL and R.M. ALFORD (1976): Synthetic seismograms: a finite-difference approach, *Geophysics*, **41**, 2-27.

KOSLOFF, D., M. RESHEF and D. LOEWENTHAL (1984): Elastic wave calculations by the Fourier method, *Bull. Seismol. Soc. Am.*, **74**, 875-899.

MARFURT, K.J. (1984): Accuracy of finite-difference and finite-element modeling of the scalar and elastic wave equations, *Geophysics*, **49**, 533-549.

MUTTI, E., J. ROSELL, G.P. ALLEN, F. FONNESU and M. SGAVETTI (1985): The Eocene Baronia tide-dominated delta-shelf system in the Ager basin, in *Excursion Guidebook: VI Eur. Reg. Mtg. IAS, Lerida, Spain, Excursion 13*, edited by M.D. MILA and J. ROSELL, 577-600.

NOAH, J.T., G.S. HOFLAND and K. LEMKE (1992): Seismic interpretation 34: seismic interpretation of meander channel point-bar deposits, *Geophysics: the leading edge of exploration*, **11** (8), 13-18.

POSTMA, H. (1967): Sediment transport and sedimentation in the estuarine environment, in *Estuaries: Am. Ass. Adv. Sci.*, edited by G.H. LAUFF, **83**, 158-179.

REBESCO, M. and A. POLONIA (1993): Modellazione monodimensionale di un sistema di barre tidali – affioramento di «Les Alteres» – Ager (Spagna), in *Atti del X Convegno Nazionale del Gruppo Nazionale di Geofisica della Terra Solida (CNR), Roma, 6-8/11/1991*, 549-560.

SELLEY, R. (1988): *Applied Sedimentology* (Academic Press Ltd. London), 86-89.

SERIANI, G. and E. PRIOLO (1991): High-order spectral element method for acoustic wave modeling, in *61st SEG Meeting, Houston (U.S.A.)*, expanded abstract, 1561-1564.

SERIANI, G., E. PRIOLO, J. CARCIONE and E. PADOVANI (1992): High order spectral element method for elastic wave modeling, in *62nd SEG Meeting, New Orleans (U.S.A.)*, expanded abstract, 1285-1288.

SERON, F.J., F. SANZ and M. KINDELAN (1987): Elastic wave propagation with finite-elements methods: comparison of different numerical techniques, in *Proceedings of the 58th SEG Annual International Meeting, Anaheim.*

WALKER, R. (1984): *Facies model*, Geoscience Canada, Geological Association of Canada, Toronto, reprint series 1, 71-89.

WIDESS, M.B. (1973): How thin is a thin bed, *Geophysics*, **38**, 1176-1180.

(received November 4, 1993;
accepted July 14, 1994)